Philosophical Magazine
Publication details, including instructions for authors and subscription information:
http://www.tandfonline.com/loi/tphm20

Size effect on the mechanical behaviour of polycrystalline copper microbeams

S. Lefebvre[a], B. Devincre[b], P. Aubert[c] & T. Hoc[ad]

[a] MSSMAT, UMR8579 ECP, Grande Voies des Vignes, 92925 Chatenay Malabry, France

[b] LEM, UMR104 CNRS-ONERA, 29 av. de la division Leclerc, 92322 Chatillon Cedex, France

[c] IEF, UMR8622, Université Paris Sud, 91405 Orsay, France

[d] LTDS, Ecole Centrale Lyon, UMR5513, 36 Avenue Guy de Collongue, 69134 Ecully, France

Published online: 02 Jun 2014.

To cite this article: S. Lefebvre, B. Devincre, P. Aubert & T. Hoc (2014): Size effect on the mechanical behaviour of polycrystalline copper microbeams, Philosophical Magazine, DOI: 10.1080/14786435.2014.914263

To link to this article: http://dx.doi.org/10.1080/14786435.2014.914263

Philosophical Magazine, 2014
http://dx.doi.org/10.1080/14786435.2014.914263

Taylor & Francis
Taylor & Francis Group

Size effect on the mechanical behaviour of polycrystalline copper microbeams

S. Lefebvre[a,1], B. Devincre[b], P. Aubert[c] and T. Hoc[a,d]*

[a]*MSSMAT, UMR8579 ECP, Grande Voies des Vignes, 92925 Chatenay Malabry, France;* [b]*LEM, UMR104 CNRS-ONERA, 29 av. de la division Leclerc, 92322 Chatillon Cedex, France;* [c]*IEF, UMR8622, Université Paris Sud, 91405 Orsay, France;* [d]*LTDS, Ecole Centrale Lyon, UMR5513, 36 Avenue Guy de Collongue, 69134 Ecully, France*

(*Received 23 January 2014; accepted 8 April 2014*)

To reduce costs and to remain competitive in the worldwide electronics industry, semiconductor manufacturers continually miniaturize devices. Today, the interconnect lines linking electronic components have diameters of the order of 100 nm or smaller. At the nanometre scale, strong size effects modify the mechanical properties of materials. To examine such effects, freestanding microbeams with geometrical and microstructural properties similar to those of interconnect lines have been designed. The yield stress dependence of the microbeams on their microstructure, shape and dimensions was investigated. As predicted by the Hall–Petch law, an increase in the yield stress with a decrease in the grain size was observed. In addition, a decrease in the cross-section of the microbeams at a fixed grain size led to a decrease in the yield stress. Hence, the yield domain of interconnect lines was observed to be controlled by two competitive size effects. This result imposes some restrictions on the design of electronic devices.

Keywords: size effect; Hall–Petch; nanostructure; copper; semiconductor

1. Introduction

The prediction of the mechanical properties of objects with submicron dimensions is a challenging problem, especially for the semiconductor industry. Indeed, Moore's law, which predicts a rapid increase in the number of components fabricated with the decrease in the size of integrated circuits, gives reason for extensive device miniaturization. Today, this trend is at the crux of technological problems such as electromigration and stress voiding, especially in the metallic interconnect lines linking electronic components. To limit these reliability problems, interconnect lines should be made of stiff materials with high yield stress and low resistivity. For this reason, interconnect lines are made of copper with a bamboo microstructure, i.e. with a single grain along the thickness and width of the lines.

In polycrystalline materials, the most referenced size effect is the Hall–Petch effect, which accounts for an increase in yield stress with a decrease in grain size, i.e. "smaller is stronger". This effect has routinely been verified experimentally in bulk materials,

*Corresponding author. Email: thierry.hoc@ec-lyon.fr
[1]Present address: ONERA, The French Aerospace Lab, 91761 Palaiseau, France.

and modelling shows that the yield stress of polycrystals with a conventional grain size increases linearly with the inverse of the square root of the grain size [1,2]. In recent years, the applicability of the Hall–Petch law to nanostructured materials has generated great interest in the scientific community. Several studies on polycrystals with grain sizes measuring a few nanometres have verified the Hall–Petch effect down to tens of nanometres, whereas for grain sizes smaller than 10 nm, a softening effect called the inverse Hall–Petch effect is observed [3,4]. The detailed knowledge of the physical processes underlying these effects is still a subject of debate. However, to date, there exists a consensus on the contributions of grain boundaries (GBs). GBs act as strong barriers to dislocation slip in large grains, whereas in nanometre-sized grains, the mechanism of GB sliding is important [5–8].

Alternatively, with a decrease in dimensions, an increase in the effect of free surfaces is observed [9–13]. Since 1979, a softening effect is known to exist when the dimensions of an object become smaller than approximately 10 times the grain size [14]. This "smaller is weaker" trend thus competes with the "smaller is stronger" Hall–Petch effect. Over the past decade, many studies on such competing geometrical effects have been carried out on polycrystals with grain sizes greater than 10 μm [15–21]. All of these studies have revealed an effect of the ratio between the sample size and the grain size, referred to as λ throughout the remainder of this study. In summary, decreasing the λ ratio leads to a decrease in the flow stress, and when λ reaches unity, the yield stress remains constant. A decrease in flow stress is typically observed for a λ ratio between 3 and 10 and depends on the material. This phenomenon is supported by the unique mechanical behaviour of grains close to a material's surface. In particular, transmission electronic microscopy (TEM) observations show that grains at the surface have a dislocation density smaller than that in the bulk [22,23].

Recently, this geometrical effect was investigated in materials with nanometre-sized grains [24–26], and a decrease in the flow stress was again observed when decreasing the λ ratio. A small increase in stress was observed in the work of Rinaldi et al. [26], but the results showed a large dispersion. This "smaller is weaker" trend can be explained through the existence of modified deformation mechanisms near a free surface in relation to GB sliding. This scenario has been partly confirmed by experiments on single-crystal nanopillars [27], in which the mechanism of GB sliding disappears. In the latter case, a decrease in the sample diameter led to an increase in the stress "due to the statistical nature of having fewer and harder dislocation sources in smaller structures" [6].

At an intermediate size scale, i.e. in materials with grain sizes between 100 nm and 10 μm, the results are more controversial. Espinosa et al. [28–30] observed a stress increase with a decrease in λ on thin films with a grain size of approximately 250 nm and a thickness varying from 200 nm to 1 μm. Chauhan [31] observed the same trend for copper-suspended thin films with thicknesses varying from 2 to 50 μm and grain sizes varying from 2 to 5 μm. Recently, Chen and Ngan [32] performed tensile tests on Ag pillars with diameters ranging from 20 to 50 μm and grain sizes ranging from 3.5 to 40 μm. In their study, Chen and Ngan reported a constant yield stress for grain sizes smaller than 20 μm, and a significant increase in yield stress with λ was observed for larger grain sizes. To justify this result, the observation of a lack of dislocation sources was reported. Finally, for large grain sizes, Yang et al. [33,34] observed a decrease in flow stress with a decrease in the λ ratio for Cu pillars with diameters ranging from 25 to 50 μm and grain sizes ranging from 3.5 to 36 μm.

The aim of the present study was to investigate the above-described λ ratio effect on the yield stress of copper interconnect lines. For such objects, the "smaller is weaker" trend is not yet well established, and to the best of the authors' knowledge, the λ ratio effect in samples with dimensions ranging from 200 nm to 1 μm and a grain size with similar dimension has not yet been investigated. We performed experiments on copper interconnect lines with a bamboo microstructure and a λ ratio close to unity. In part 2, the material and the bending test we used are described. Then, the yield stress results are presented in part 3 and discussed according to the evolution of the λ ratio in part 4.

2. Experimental method

To study the effects of interconnect lines geometries (width and thickness) and dimensions on mechanical properties, particularly the yield stress, bending tests were performed using a nanoindentor device. The bending samples we used were copper microbeams fixed at both ends, which were fabricated using conventional technology by Altis Semiconductor.

2.1. *Suspended microbeam manufacture*

In this section, the production of the suspended bending samples, i.e. submicron parallel copper freestanding microbeams fixed at both ends [35], is described. The starting point of the manufacturing process is a support silicon wafer with a standard diameter of 200 mm. After cleaning the substrate by a conventional method, a silicon nitride film measuring approximately 50–100 nm thick was deposited. This first layer reduced the mechanical stresses induced by the silicon wafer and the upper deposited thin films. Then, a layer with a thickness of approximately 3 μm used to create the void space was deposited. This layer was selected to have an etching rate of one order of magnitude greater than the etching rates of the other materials involved in the manufacture of the microbeams. Finally, a second silicon nitride transfer layer measuring approximately 450 or 800 nm in thickness was deposited on the void layer.

In the second step, the transfer layer of the copper microbeams was patterned. A resin mask featuring holes in the shape of the engineered microbeams was deposited on the transfer layer. This layer was then etched using an ultraviolet lithographic process to reproduce the mask pattern. Next, a 20 nm copper seed layer was deposited by physical vapour deposition, and a layer of copper was electrochemically deposited to completely fill the grooves. Excess copper was then removed using a chemical–mechanical polishing (CMP) process. Annealing (using industrial conditions) was then carried out to promote grain growth. All process parameters used in this procedure followed those actually used in industrial processes to ensure the best interconnect lines performance.

Etching of the oxide under and around the deposited copper was the last step of manufacturing. This process followed the same steps used for copper deposition but with modified photolithography and etching procedures. The portion of the layer under and around the microbeams was exposed by a combination of wet and dry etching. Dry etching allows for the control of the direction of etching and can thus be used for anisotropic or isotropic etching. In the present work, anisotropic etching was used to etch along the vertical direction only, whereas isotropic etching was to etch in all directions, in particular, along the depth direction and laterally. Finally, the residual material under

the copper microbeams was removed by isotropic wet etching. Therefore, a combination of two types of etching was required to create the cavity needed to suspend the microbeams used as bending samples.

A typical example of the microbeam samples is shown on Figure 1. It is worth noting that five parallel microbeams in a closed area with the same geometrical specificity were systematically patterned. In the present study, 12 different microbeam geometries with widths of 280, 380, 500, 600, 800 and 900 nm and thicknesses of approximately 450 and 800 nm were fabricated. The geometry of the 60 elaborated microbeams was systematically verified by scanning electron microscopy (SEM) imaging.

2.2. *Measurement of microbeam thickness*

Accurate measurements of the thickness of the copper microbeams were performed using the four-point electrical resistivity method. This method is a non-destructive reliable industrial method used to determine the thickness of a metal layer after CMP. The measurements were conducted with the help of specific devices included in the copper microbeam deposition mask. The devices were similar in shape to the copper microbeam bending samples, with widths ranging from 440 to 740 nm, and were connected to four square contact panels (see Figure 2).

For the resistivity measurements, tungsten carbide tips were placed on the four panels. A current was injected between the two most external panels, and the voltage was measured between the two remaining panels. A value for the electrical resistance R was then determined with an accuracy of 5–10%. In the present study, the reported measurements were performed using an Agilent 4156 parameter analyser with a ramp voltage from −1 to +1 V. Based on the resistivity measurements, the thickness of the microbeams, h, was derived from the standard equation:

$$h = \frac{L\rho}{RW}$$

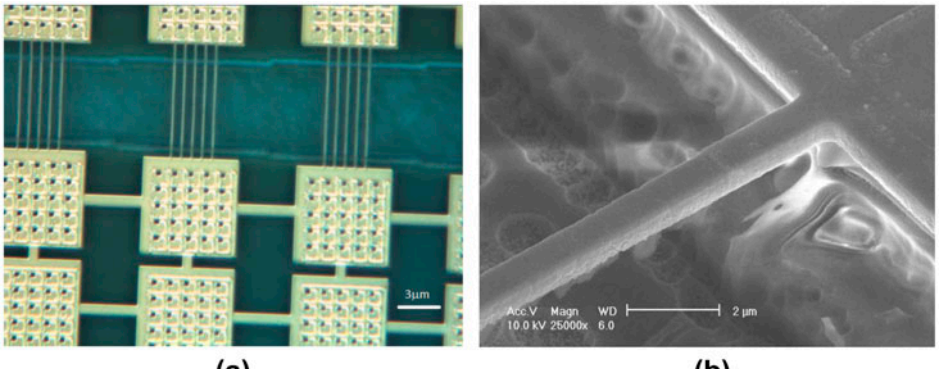

Figure 1. (colour online) (a) Optical image of 3 sets of five suspended beams. The two parallel white lines perpendicular to the beams correspond to the trench created by etching to suspend the microbeam. (b) SEM image of a microbeam, 800 nm wide, 450 nm thick and 8 µm long, observed at an accelerating voltage of 10 kV, a magnification of 25,000 and a tilt of 35°.

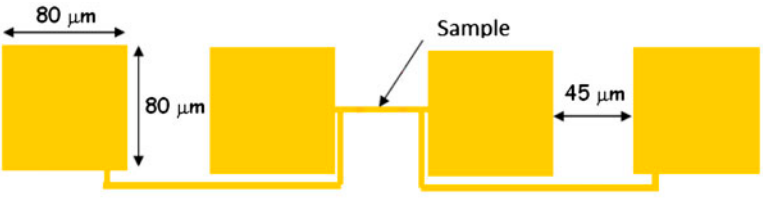

Figure 2. (colour online) Design of the four-point electrical resistivity pattern included in the deposition mask and used to measure the thickness of the microbeams.

where L and W are, respectively, the length and the width of the microbeams. The electric resistivity of the microbeams, ρ, was not determined in the present study; instead, a value of $2 \times 10^{-8}\,\Omega\,\mathrm{m}$ was assumed (Altis Semiconductor internal data). The thickness of the four microbeams was double checked by direct SEM observation. The difference between SEM and resistivity measurements was found to always be less than 5%.

2.3. *Metallurgical characterization of microbeams*

Secondary ion mass spectrometry was used to determine the microbeam composition. A selected microbeam measuring 450 nm thick was analysed with a CAMECA IMS 6F device, using a caesium source, a current of 15 nA, a primary acceleration voltage of 10 kV and a negative secondary acceleration voltage of −4500 kV. This analysis confirmed that the primary element of the tested microbeams was copper, but the presence of significant amounts of chlorine, carbon and oxygen was observed.

Texture measurements were performed using electron backscattering diffraction with a Leo 1530 FEG-SEM. Crystallographic orientations were carried out using the Orientation Imaging Microscopy TSL analysis software. Orientation mapping of the beams' top surface was made with incremental steps of 0.1 μm in the lateral and the longitudinal directions. Due to the small number of grains into the beams and due to difficulty in performing EBSD measurement on fine samples, the standard microstructure of beams was determined by sampling 10 beams of dimensions 400 nm wide and 450 nm thick, and 10 beams of dimensions 800 nm wide and 800 nm thick. The microbeams used in this analysis were still embedded and all showed a fibre texture with grains oriented either along the {1 1 1} or {1 0 0} planes. The volume fractions of the {1 1 1} and {1 0 0} fibres were approximately 55 and 45%, respectively. Based on this EBSD analysis, average grain sizes of 400 and 600 nm were measured for the microbeams with thicknesses of 450 and 800 nm, respectively.

In addition, the grain morphology of the microbeams was analysed using TEM. Regardless of the microbeam geometry, TEM images revealed a bamboo microstructure with parallel and equidistant GBs along the bending sample length (Figure 3(c) and (d)). The latter observations are consistent with the results of the EBSD analysis. Hence, the microbeam samples tested in this study were composed of polycrystalline copper with adjacent cuboid grains. The grains dimensions were determined by the width and the thickness of the microbeams.

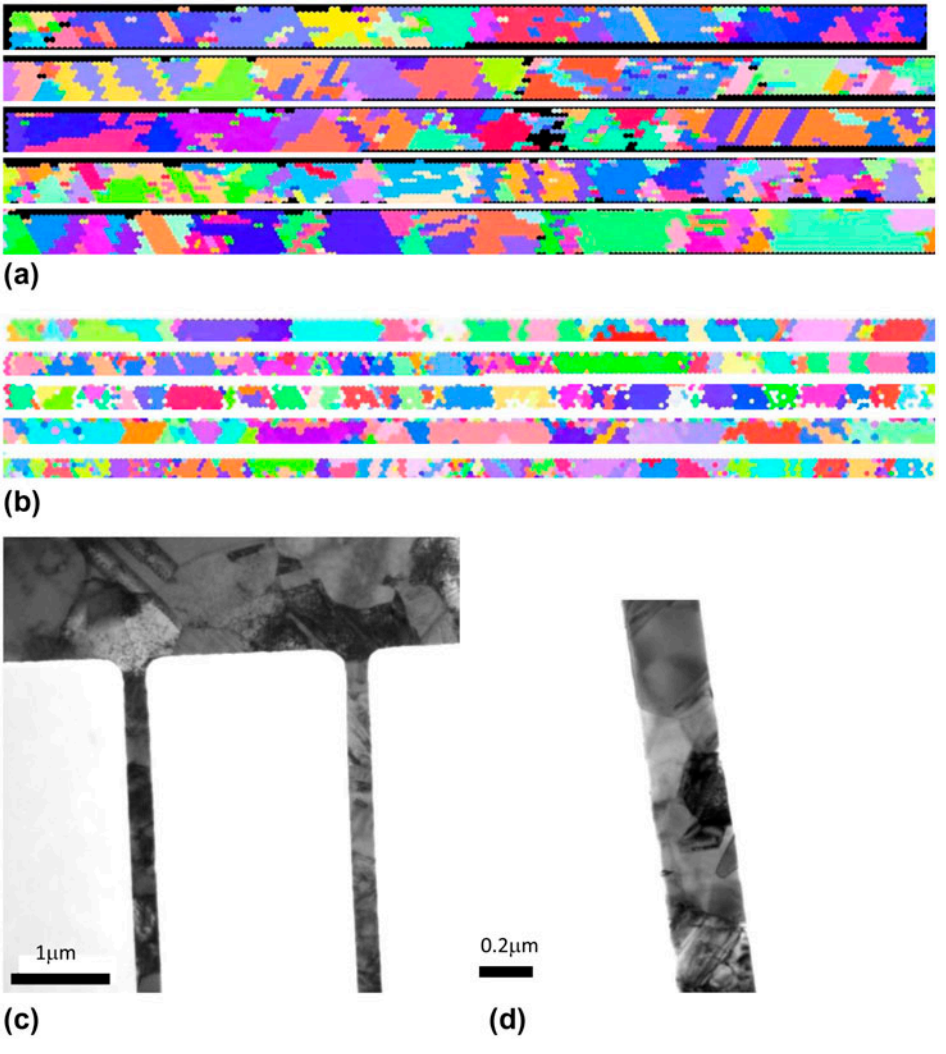

Figure 3. (colour online) Morphological grain size analysis on the top of the beam. (a) Grain orientations obtained by EBSD of five microbeams measuring 800 nm wide and 800 nm thick; (b) grain orientations obtained by EBSD of five microbeams measuring 400 nm wide and 450 nm thick; (c) and (d) microstructure of microbeams measuring 280 nm wide and 450 nm thick obtained by TEM.

2.4. *The micro-bending test procedure*

Bending tests were performed at the University of Evry using a Veeco Dimension 3100 atomic force microscope combined with a Hysitron nanoindentation apparatus. The main advantage of this device is its accuracy in lateral position resolution (20 nm) and its ability to image and to indent samples with the same tip. In the present study, a Berkovich tip with an average radius of curvature of 150 nm was used. To account for the device stiffness, the method described by Holbery et al. [36] was used. This method

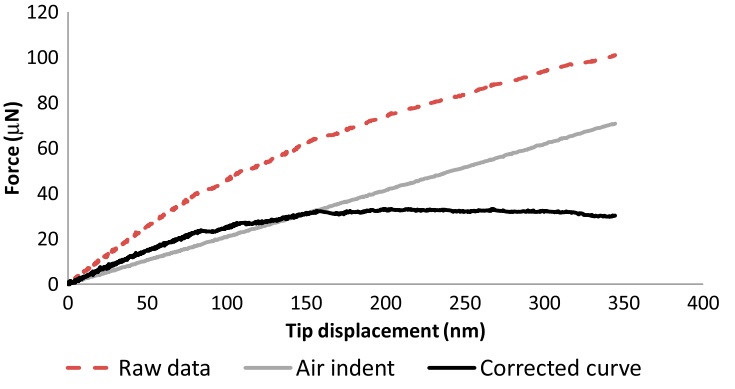

Figure 4. (colour online) Typical curves obtained by the nanoindentation test. The dashed line corresponds to the raw data obtained during microbeam sample bending. The grey line corresponds to the nanoindentation test performed without a sample. The black line is the corrected force–displacement curve obtained by subtracting the two previous curves.

consists in performing a nanoindentation test first in air before touching the bending sample. Then, subtracting the two monitored signals gives a precise calculation of the effective force applied to the samples (see, for instance, Figure 4).

The same bending test methodology was used for all of the tested microbeams. Bending was induced by imposing a force load proportional to time with a strength rate equal to 2.33 $\mu N\,s^{-1}$. Before loading, the apparatus's AFM mode can be used to precisely localize one microbeam centre in a set of five parallel bending samples. From this initial location, the coordinates of the five adjacent microbeam centres can be calculated, and five nanoindentation loads can be automatically performed.

In all the bending tests, the indenter tip penetrated the microbeam samples during loading. To quantify the effect of this penetration, a nanoindentation test was performed on a copper thin film measuring 450 nm in thickness fabricated by the same manufacturing process. The hardness of this thin film was determined to be approximately 1.5 GPa. The tip penetration depth recorded on this thin film at 3 and 35 μN were approximately 0.6 and 7 nm, respectively. The indenter penetration depth was therefore always very small compared to the thickness of the microbeam samples.

3. Results

3.1. *Sample thickness*

The times of etching considered in the deposition method led to expected thicknesses of 450 and 800 nm. The true thickness of the samples was confirmed using the four-point resistivity procedure on four wide patterns measuring 440, 540, 740 and 940 nm. The measured mean thicknesses for the 450 and 800 nm samples were 433 ± 13 and 779 ± 17 nm, respectively. In both cases, the measured thickness was slightly smaller than the expected one. The difference was approximately 3%.

3.2. *Sample yield force and elastic stiffness*

A typical force–displacement curve is reproduced in Figure 5(a). This curve corresponds to the bending test performed on microbeams measuring 380 nm in width and

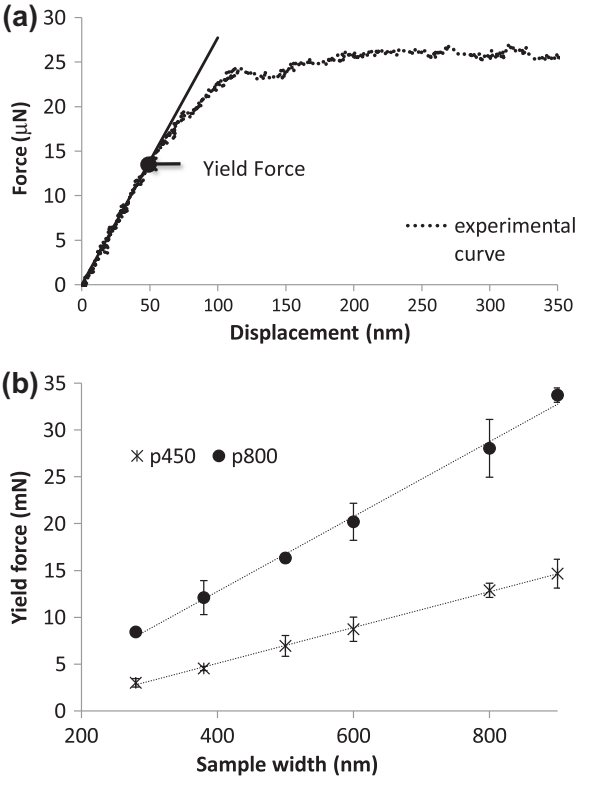

Figure 5. (a) Typical force–displacement curve for beams measuring 380 nm wide and 800 nm thick. (b) Yield forces measured for the 12 geometries of samples. For each point, the standard deviation was obtained using four samples of the same geometry. The black circle corresponds to 800 nm-thick samples and the cross symbol to 450 nm-thick samples.

800 nm in thickness. All of the force–displacement curves obtained can be decomposed into two parts: (i) a linear part corresponding to the elastic domain and (ii) a non-linear part featuring significant plastic deformation. As conventionally reported, the inflection point at the boundary between the linear and non-linear domains is defined as the yield force. In Figure 5(b), the average values of the yield force measured with different geometries of microbeam samples are reported. Each value is the average of at least four bending test measurements. The yield force varied from 3 μN for the microbeams measuring 280 nm wide and 450 nm thick to 35 μN for the microbeams measuring 900 nm wide and 800 nm thick. Moreover, the yield force increased linearly with the microbeam width and thickness. The error bars plotted in Figure 5(b) are plus and minus one standard deviation of the measurements made for samples having the same geometry. Attention should be drawn to the small magnitude of the obtained error bars.

The calculations of the elastic stiffness for the 12 tested microbeam geometries, i.e. the slope of the force–displacement curve in the elastic domain, are summarized in Figure 6. The elastic stiffness varies from 43 $\mu N\,nm^{-1}$ for the microbeams measuring 280 nm wide and 450 nm thick to 710 $\mu N\,nm^{-1}$ for the microbeams measuring 900 nm

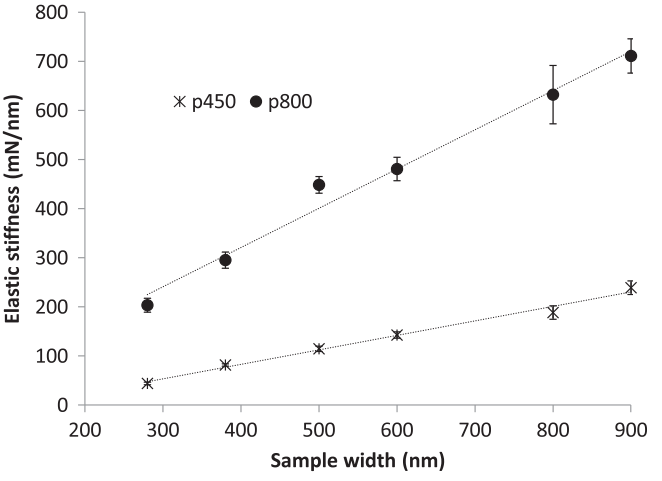

Figure 6. Elastic stiffness for the 12 investigated sample geometries. For each point, the standard deviation was calculated using four samples with the same geometry. The black circle corresponds to 800 nm-thick samples and the cross symbol to 450 nm-thick samples.

wide and 800 nm thick. Similarly, to the yield force, the elastic stiffness increased linearly with the sample width and was higher for the thicker microbeam samples. The calculated mean values again exhibit a small standard deviation. These two results demonstrate the excellent reproducibility of the experimental procedure developed in the present study. In addition, it is worth noting that the large elastic stiffness variation measured is related only to the modification of the size and geometry of the tested samples.

3.3. *Sample yield stress*

The stress field associated with the bending test is not uniform and consequently does not allow for the direct determination of samples' yield stress. In the present study, reverse finite element method (FEM) simulations that reproduce the experimental force–displacement curves were systematically performed to calculate the samples' yield stress. This process involved two steps. First, the geometry of the microbeam samples was precisely determined, and second, the yield surface domain of a standard plastic law was identified to reproduce the experimentally measured force–displacement curves.

Because the etching procedure used to manufacture the samples removes the material around the microbeams and also under the anchor square devices that support the microbeams, close attention must be paid to the calculation of the sample geometry after fabrication. Figure 7 shows a cross-section of one anchor square at some distance from the microbeam contact area. The SEM image shows the presence of an engraved volume under the anchor square. Hence, the boundary between the anchor square device and the end of the microbeam, i.e. geometry and built-in end, is poorly defined. Thus, simulations were needed to determine the effective length of the tested microbeam samples.

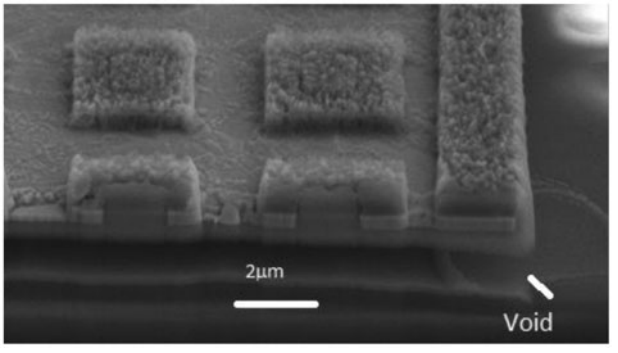

Figure 7. SEM image of an anchor square device supporting the microbeam samples. Even far from the microbeam contact region (top right part of the image), one can observed a significant engraved void under the anchor square device.

For each experimental bending test, finite element simulations were performed with the finite element code Abaqus 6.9.2. The FE mesh was composed of at least four cubic linear elements (C3D8) along the smallest dimension of the microbeam. The boundary conditions were fixed at the microbeam ends, and displacement was imposed in the middle of the sample length. The substrate was assumed perfectly rigid. For simplicity, the constitutive materials property law used for the computations was assumed to be isotropic, linear-elastic/ideally plastic and characterized by three parameters: the Young's modulus E set to 125 GPa, Poisson's ratio v set to 0.3 and the von Mises yield stress Y_{id}. In the first step, the microbeam length used in the finite element simulation was modified until the sample elastic stiffness measured was reproduced. In a second step, the yield stress value was identified to obtain a numerical yield force consistent with each experimental measurement. The latter calculation was of course performed by considering the effective sample length determined in the first calculation step.

The mean values of the effective microbeam length we obtained for the microbeams measuring 450 and 800 nm in thickness were, respectively, $9.9\,\mu m \pm 0.25$ and $9\,\mu m \pm 0.75$. As expected, these values are longer than the 8 µm initially designed in the etching mask. This result demonstrates the strong effect of the etching step during sample preparation. The results of the yield stress calculations are reported in Figure 8, which shows that the thinner microbeams exhibited a higher yield stress. More precisely, a constant increase of approximately 36 MPa was observed when reducing the microbeam thickness from 800 to 450 nm at a fixed width. Conversely, the yield stress increased linearly with the width of the microbeams at constant thickness.

4. Discussion

In this study, the yield stress of microbeams fabricated using materials and processes employed in actual interconnects was determined. To this end, an innovative and reproducible methodology was developed to create ultrafine copper microbeams [35]. Bending tests in conjunction with nanoindentation measurements were then performed on a large set of samples with different widths and thicknesses. Good reproducibility of the bending

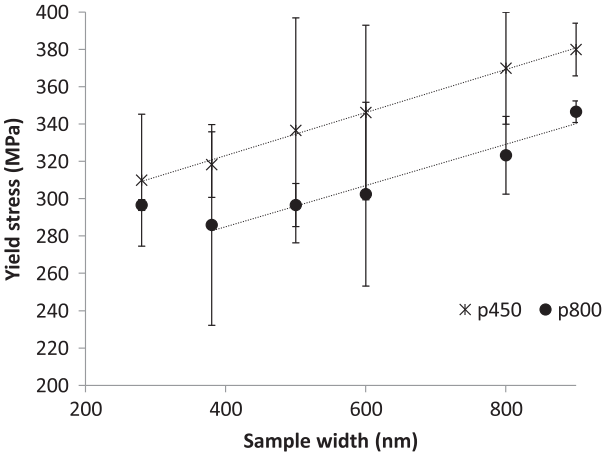

Figure 8. Yield stress obtained for the 12 sample geometries. The sample measuring 280 nm wide and 800 nm thick was not taken into account in the linear regression fit. For the 450 nm-thick sample, the linear fit equation is $\sigma = 0.11$ width $+ 276$ ($R^2 = 0.99$), and that for the 800 nm-thick sample is $\sigma = 0.11$ width $+ 240$ ($R^2 = 0.95$).

results was achieved for microbeam samples with widths ranging from 900 nm down to 280 nm. The yield stress values obtained were between 280 and 380 MPa and are consistent with the results reported by Schwaiger [37] for copper thin films deposited on a polyimide substrate. Schwaiger observed a yield stress of 290 MPa for films measuring 800 nm thick and a yield stress of 325 MPa for films measuring 400 nm thick. It is interesting to note that the strengthening value of 35 MPa observed in [37] with decreasing film thickness compares very well with the value of 36 MPa measured in the present study when decreasing the microbeam thickness from 800 to 450 nm.

All calculations were performed by considering isotropic elasticity, whereas copper is a strongly anisotropic material. To justify this simplification, using FEM simulations, we calculated the elastic properties of a copper polycrystal composed of 27,000 grains and reproduced the crystallographic texture of the microbeams (i.e. 55% of grains oriented along the ⟨1 1 1⟩ directions and 45% of grains oriented along the ⟨1 0 0⟩ directions). Considering the elastic constants of Cu, $C_{11} = 168$ GPa, $C_{12} = 121.4$ GPa and $C_{44} = 75.4$ GPa, the apparent Young's moduli calculated in the x, y and z directions are, respectively, 127.1, 126.9 and 126.9 GPa. This simple calculation shows that the texture existing in the microbeams justify the isotropic elasticity calculations. Nevertheless, the small number of grains inside the microbeams, which showed a bamboo microstructure, could modify the aforementioned analytical results. To test for this possibility, we used the FEM to simulate the bending tests performed on five microbeams with a constant thickness of 450 nm and accounted for the real sample microstructures identified by the EBSD technique (see Figure 3(b)). In the simulations, the elasticity was considered anisotropic and each grain was ideally plastic with the same von Mises yield stress. The variation in the yield force between the five simulations was always less than 10%. This result is consistent with the weak standard deviation of yield forces observed experimentally. From the two calculations, we concluded that it is satisfactory to describe the microbeams as being isotropically elastic.

In the present study, special care was taken to fabricate microbeam samples highly similar to actual interconnects. Both have a bamboo microstructure and feature dimensions smaller than one micrometre. With these micron-sized samples, it is possible to perform bending tests and to study the size effects associated with the geometry and dimensions of actual interconnects. In the literature, it is reported that in samples with dimensions greater than 10 µm, a decrease in the ratio λ between one sample dimension to the grain size leads to a decrease in yield stress. This size effect is frequently attributed to the modification of the plastic properties of grains close to a free surface. Surprisingly, the important case of interconnects with a λ ratio close to unity and with a sub-micrometre grain size has not yet been investigated systematically.

The complex size effect observed is summarized in Figure 9. In this figure, the normalized yield stress Y_{id}/Y_o versus the ratio λ of the average transverse dimension of the microbeam sample to its grain size is plotted. Here, the sample reference dimension is defined as the average of the side lengths $(T+W)/2$, where T and W are the thickness and the width of the microbeams, respectively [34]. Y_o is the thin film yield stress, named Y_o^{450} and Y_o^{800} for thin film of 450nm and 850nm thick, respectively. In the present analysis, Y_o^{450} was calculated by performing a nanoindentation test on a 450 nm copper thin film fabricated under the same conditions used to create the microbeams (see Section 2.4). For this calculation, the following standard equation [24] was used:

$$H = M \cdot Y_o$$

where H is the indentation hardness and M the classical Tabor factor, which is equal to 3. Based on this equation, Y_o^{450} is approximately 0.5 GPa in films with a thickness equal to 450 nm. In accordance with the results shown in Figure 8, the value of Y_o^{800} for the films measuring 800 nm in thickness was assumed to be $Y_o^{800} = Y_o^{450} - 0.036$ GPa = 0.5–0.036 GPa.

The results reported in Figure 9 are quite similar to those obtained for other types of samples with larger dimensions [14,17–21]. A decrease in the normalized yield stress

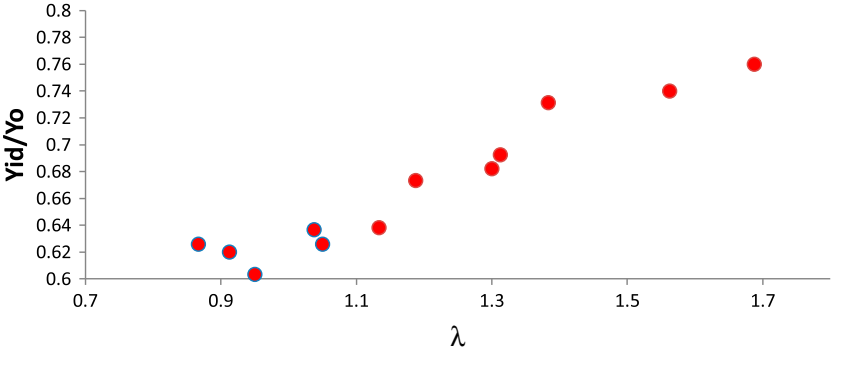

Figure 9. (colour online) Normalized yield stress with respect to the ratio of the lateral average size of samples to their grain size. This plot includes results obtained for microbeams with widths ranging from 900 nm down to 280 nm and a thickness of 800 or 450 nm.

is observed with the decrease in the λ ratio. Below a value close to 1, the normalized yield stress is observed to be constant. It is interesting to note that Keller and Hug [19] already observed such yield-saturating behaviours but in polycrystalline nickel samples with much larger dimensions in the range 3.2 mm–12.5 μm.

The elementary mechanisms controlling the size effect in the present study appear to be relatively straightforward. Considering the effect of the image force on dislocations, which is strong at distances smaller than 500 nm from a free surface, dislocations in regions close to the sample surfaces are easily eliminated. Thus, a decrease in the dislocation density that makes plastic deformation easier in the absence of dislocation source starvation is expected. Conversely, dislocation storage and Hall–Petch strengthening is believed to take place in the regions close to GBs. Hence, as a consequence of the microbeams' bamboo microstructure, changing the sample lateral dimensions to increase λ is equivalent to reducing the fraction of grain boundary at the samples' free surfaces. The size effect observed on the yield stress, therefore, results from a competition between this free surface effect, which dominates at values of λ that are close to unity, and GB strengthening at larger values of λ.

To conclude, a method for characterizing the mechanical properties of copper interconnects based on bending tests of freestanding microbeams has been proposed. Reducing the sample thickness increases the yield stress, and reducing the width decreases the yield stress. The evolution of the yield stress as function of λ, i.e. the ratio of the average transverse dimension of samples to the grain size, helps explain the physical origin of the observed size effects existing in copper interconnects. We showed that in the particular case of copper polycrystalline microbeams with lateral dimensions and a grain size ranging from approximately 1.0 to 0.2 μm, the microbeam yield stress decreases with λ. This behaviour is consistent with other observations made for samples with dimensions larger than 10 μm or smaller than a few tens of nanometres. Thus, the present study highlights the existence of a non-trivial size effect in interconnect devices commonly used in the semiconductor industry. In agreement with other previous studies on thin films, micropillars or other model sample geometries, the yield stress of interconnect lines is controlled by the competition between two size effects. For this reason, the optimization of the mechanical properties of interconnects requires that the shape of the interconnects be designed such that the λ ratio, GB size and free surface area are as large as possible.

Acknowledgements

The support of Altis Semiconductor and Elastic GB [grant number ANR-09-BLAN-0079] for this research project is acknowledged. The authors gratefully acknowledge Ladisla Kubin and Olek Maciejak for their helpful discussions. The authors are also grateful to Pierre Vekeman, Daniel Bertrand and Pascal Deconinck from Altis Semiconductor for their support and technical assistance.

References

[1] E.O. Hall, Proc. Phys. Soc. London, Sect. B 64 (1951) p.747.
[2] J. Petch, J. Iron Steel Inst. 174 (1953) p.25.
[3] V.Y. Gertsman, M. Hoffmann, H. Gleiter and R. Birringer, Acta Metall. Mater. 42 (1994) p.3539.

[4] P.G. Sanders, J.A. Eastman and J.R. Weertman, Acta Mater. 45 (1997) p.4019.
[5] M. Dao, L. Lu, R.J. Asaro, J.T.M. Dehosson and E. Ma, Acta Mater. 55 (2007) p.4041.
[6] J.R. Greer and J.Th. De Hosson, Prog. Mater. Sci. 56 (2011) p.654.
[7] S. Lefebvre, B. Devincre and T. Hoc, Mater. Sci. Eng. A 400–401 (2005) p.150.
[8] S. Lefebvre, B. Devincre and T. Hoc, J. Mech. Phys. Solids 55 (2007) p.788.
[9] E. Arzt, Acta Mater. 46 (1998) p.5611.
[10] C.Q. Sun, Prog. Mater. Sci. 54 (2009) p.179.
[11] G.A. Malygin, Phys. Solid State 54 (2012) p.559.
[12] J. Gong and A.J. Wilkinson, Acta Mater. 59 (2011) p.5970.
[13] D. Kiener, C. Motz, T. Schöberl, M. Jenko and G. Dehm, Adv. Eng. Mater. 8 (2006) p.1119.
[14] S. Miyazaki, K. Shibata and H. Fujita, Acta Metall. 27 (1979) p.855.
[15] T.A. Kals and R. Eckstein, J. Mater. Process. Technol. 103 (2000) p.95.
[16] L.V. Raulea, A.M. Goijaerts, L.E. Govaert and F.P. Baaijens, J. Mater. Process. Technol. 115 (2001) p.44.
[17] P.J.M. Janssen, Th.H. de Keijser and M.G.D. Geers, Mater. Sci. Eng., A 419 (2006) p.238.
[18] A. Molotnikov, R. Lapovok, C.H.J. Davies, W. Cao and Y. Estrin, Scr. Mater. 59 (2008) p.1182.
[19] C. Keller and E. Hug, Mater. Lett. 62 (2008) p.1718.
[20] S. Mahabunphachai and M. Koc, Int. J. Mach. Tools Manuf. 48 (2008) p.1014.
[21] C. Keller, E. Hug and X. Feaugas, Int. J. Plast. 27 (2011) p.635.
[22] H. Mughrabi, Phys. Status Solidi B 39 (1970) p.317.
[23] C. Keller, E. Hug, R. Retoux and X. Feaugas, Mech. Mater. 42 (2010) p.44.
[24] X. Gu, C. Loynachan, Z. Wu, Y. Zhang, D. Srolovitz and J. Greer, Nano Lett. 12 (2012) p.6385.
[25] D. Jang and J.R. Greer, Scr. Mater. 64 (2011) p.77.
[26] A. Rinaldi, P. Peralta, C. Friesen and K. Sieradzki, Acta Mater. 56 (2008) p.511.
[27] M.D. Uchic, D.M. Dimiduk, J.N. Florando and W.D. Nix, Science 305 (2004) p.986.
[28] H.D. Espinosa, B.C. Prorok and M. Fischer, J. Mech. Phys. Solids 51 (2003) p.47.
[29] H.D. Espinosa, B.C. Prorok and B. Peng, J. Mech. Phys. Solids 52 (2004) p.667.
[30] H.D. Espinosa, M. Panico, S. Berbenni and K.W. Schwarz, Int. J. Plast. 22 (2006) p.2091.
[31] S. Chauhan and A. Bastawros, Appl. Phys. Lett. 93 (2008) p.041901.
[32] X. Chen and A.H.W. Ngan, Scr. Mater. 64 (2011) p.717.
[33] B. Yang, C. Motz, W. Grosinger and G. Dehm, Procedia Eng. 2 (2010) p.925.
[34] B. Yang, C. Motz, M. Rester and G. Dehm, Philos. Mag. 92 (2012) p.3243.
[35] P. Vekeman, S. Lefebvre, T. Hoc and P. Deconinck, Patent No. US-7,754,506 B2 (2010).
[36] J.D. Holbery, V.L. Eden, M. Sarikaya and R.M. Fisher, Rev. Sci. Instrum. 71 (2000) p.10.
[37] R. Schwaiger, *Fatigue behavior of sub-micron silver and copper films*, Ph.D. thesis, Universität Stuttgart, 2001.